ISSN 1995-0780, Nanotechnologies in Russia, 2020, Vol. 15, Nos. 11–12, pp. 701–707. © Pleiades Publishing, Ltd., 2020.
Russian Text © The Author(s), 2020, published in Rossiiskie Nanotekhnologii, 2020, Vol. 15, No. 6, pp. 733–740.

SELF-ASSEMBLED STRUCTURES AND NANOASSEMBLIES

$Pt/Ti_{1-x}Ru_xO_{2-\delta}$ Cathodic Electrocatalysts for Fuel Cells

A. A. Belmesov[a,*], A. V. Levchenko[a], A. A. Baranov[a,b], S. E. Nadkhina[a], and A. P. Melnikov[a,b,c]

[a] *Institute of Problems of Chemical Physics, Russian Academy of Sciences, Chernogolovka, Moscow Region, 142432 Russia*
[b] *Lomonosov Moscow State University, Moscow, 119991 Russia*
[c] *Moscow Institute of Physics and Technology, Dolgoprudny, Moscow Region, 141701 Russia*
**e-mail: belmesovaa@mail.ru*

Received June 16, 2020; revised August 26, 2020; accepted August 31, 2020

Abstract—In this paper, we study the electrocatalytic activity and stability of materials in the $Pt/Ti_{1-x}Ru_xO_{2-\delta}$ system, in oxygen electroreduction reactions, including under operating conditions in a fuel cell (FC). All the obtained electrocatalytic materials are shown to be stable in the electrode potential range of operation of a hydrogen-air FC, while the electroreduction of oxygen proceeds mainly by a four-electron mechanism. The power characteristics of the FC with the obtained electrocatalyst are comparable to those of a FC with a commercial electrocatalyst, while the stability of the obtained electrocatalysts is 5–6 times higher than that of Pt/C catalysts.

DOI: 10.1134/S199507802006004X

INTRODUCTION

Electroreduction of oxygen at the cathode of a fuel cell (FC) is usually a slower process than most anodic reactions. For example, the apparent exchange current density for the oxygen reduction reaction (ORR) is $i_{cathode} \sim 6$ μA/cm^2 [1], which is several orders of magnitude less than that for the hydrogen oxidation reaction, which is $i_{anode} \sim 0.1$ A/cm^2. Besides, intermediate products, which activate corrosion processes on electrode materials, are formed at the cathode. In this regard, the service life and operating characteristics of FCs are largely determined by the electrochemical parameters of the cathode catalytic layer [2]. The main cathodic process in a hydrogen-air fuel cell is the ORR:

$$2H^+ + 2e^- + 0.5O_2 = H_2O_{(l)}. \quad (1)$$

The efficiency of energy conversion in fuel cells is mostly determined by the kinetic hindrances of this process [3]. In accordance with [3] (Fig. 1), the ORR mechanisms on Pt include several separate reactions. First, oxygen can be directly reduced to H_2O in an acidic electrolyte with the addition of four electrons (direct ORR). Another way of O_2 reduction includes the intermediate H_2O_2 formation without breaking the O–O bond (by the two-electron mechanism) and the subsequent conversion of hydrogen peroxide. For an application in fuel cells, the most effective ORR catalysis is the oxygen reduction to water molecules via the four-electron path.

Incomplete reduction of O_2 to H_2O_2 not only leads to low efficiency of energy conversion, but can also produce free radicals that activate the oxidation processes of electrode materials, primarily carbon support, and membrane [4].

An increase in catalytic activity in ORR can be achieved by using platinum alloys, since the OH_{ads} formation on Pt atoms can be inhibited on their surface due to the combined effect of the surface geometry and electronic structure [5]. According to [6], the potential of the onset of OH_{ads} adsorption on alloys can shift to more positive potentials (for Pt/C, this value is usually higher than 0.8 V) [7].

To increase the catalytic activity of cathode catalysts, it is important to focus on the creation of materials that activate the ORR proceeding along the four-electron pathway and that are stable to oxidation. The support of the electrocatalyst must meet the following requirements: be uniform throughout the volume (with a narrow particle size distribution) and have high electrical conductivity [8].

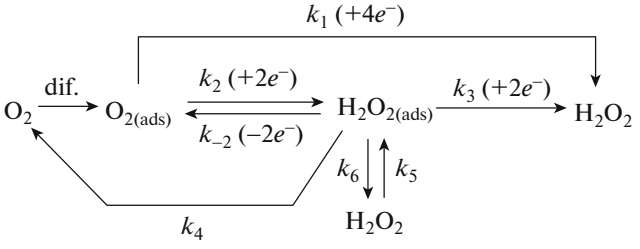

Fig. 1. Diagram of the mechanism of oxygen reduction on Pt catalysts [2].

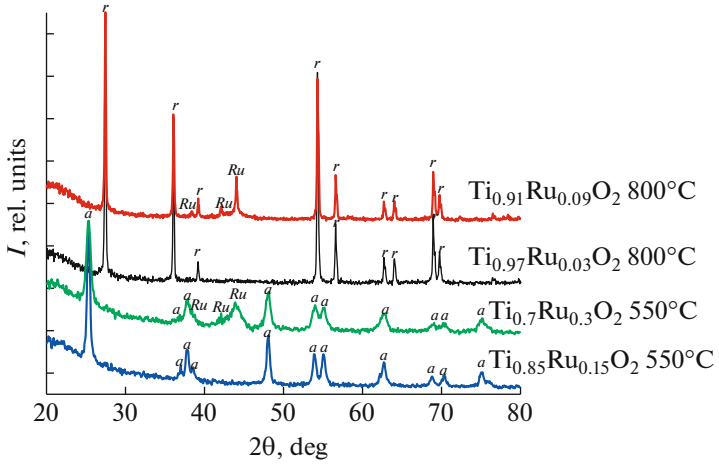

Fig. 2. (Color online) X-ray diffraction patterns of catalyst support samples. Symbol *a* marks reflexes of anatase, symbol *r* marks reflexes of anatase rutile, and symbol Ru marks reflexes of metallic ruthenium.

To increase the stability to oxidative degradation, many researchers modify the carbon supports of catalysts or replace them with other types of supports, in particular, various metal oxides, for example, SnO_2 [9], TiO_2 [10], and MoO_x [11]. At present, there are publications in which titanium oxide is used as a support material for electrocatalysts [8, 12–14]. This choice is due to the high chemical and electrochemical stability in an acidic medium, the low cost of titanium oxide, and the possibility of its use in the form of a highly dispersed powder. As was noted in [15, 16], when titanium oxide is doped with ruthenium oxide or niobium oxide, a significant increase in the oxide support conductivity up to about 1×10^{-4} S/cm at a dopant content of 7–8 mol % is observed.

EXPERIMENTAL

Oxide supports with a composition $Ti_{1-x}Ru_xO_{2-\delta}$, where $x = 0$–0.3 (0 mol % ≤ Ru ≤ 30 mol %) were synthesized by precipitation from an alcohol solution of $Ti(OBu)_4$ (Acros Organics 99%) and $RuCl_3$ (chemically pure) with an aqueous solution of nitric acid (chemically pure). The resulting gel was left to mature at room temperature for a week, then the solvent residue was removed using a porous glass filter, and the precipitate was washed [17, 18]. The resulting dry precipitate was annealed in air at 300°C, then in hydrogen at 550°C to obtain samples with anatase structure, and at 800°C to obtain samples with rutile structure [19]. After annealing the samples containing 0–3 mol % Ru in hydrogen at 800°C, the X-ray diffraction pattern obtained with a DRON-UM2 powder diffractometer (Russia) contains only peaks of the rutile phase while the X-ray diffraction pattern of samples with a Ru content of ≥4 mol % shows also peaks related to the metallic ruthenium phase (Fig. 2). After annealing the samples containing 0–15 mol % Ru in hydrogen at 550°C, the X-ray diffraction pattern contains peaks of the anatase phase while the X-ray diffraction pattern of samples with a Ru content of 30 mol % also shows peaks related to the metallic ruthenium phase (Fig. 2). All the obtained samples were used for further studies.

The specific surface area of oxide supports was determined by the BET method by nitrogen desorption using a NOVA 3200 instrument (Quantachrome Instruments, USA). The conductivity of oxide supports was measured in a four-zone cell.

Platinum was deposited on an oxide substrate by reduction of H_2PtCl_6 with ethylene glycol (Sigma Aldrich), which acted as a solvent and reducing agent [17]. The platinum content in the obtained samples was determined by X-ray fluorescence analysis (X-Art M, KOMITA, Russia) and energy dispersive X-ray microanalysis (LEO SUPRA 25, Carl Zeiss, Germany). Micrographs (Fig. 3a) obtained with a LEO SUPRA 25 scanning field emission electron microscope (Carl Zeiss, Germany) showed that platinum is uniformly distributed over the oxide surface, and the average particle size is 4–6 nm.

The electrochemically active surface area of platinum deposited on oxide substrates was determined by the desorption of hydrogen (S_{sp_H} Pt), carbon monoxide (S_{sp_CO} Pt), and copper adatoms (S_{sp_Cu} Pt) [17, 20] (Fig. 4). To increase the conductivity (up to $\sigma = 3 \times 10^{-2}$ S/cm), carbon nanotubes (CNTs) [21] of ~ 5 wt % (a diameter is 1–5 nm, $S = 280$ m^2/g) were added to the samples, the conductivity of the composites is described in [22]. We used a disk electrode made of glassy carbon and isotropic pyrocarbon (S_e = 0.196 cm^2). The catalyst in the form of an extremely thin layer of "catalytic ink," which was prepared as follows, was applied to the electrode: 10 mg of the studied catalyst with 20 μL of a 10% Nafion solution in 1 mL of isopropyl alcohol was sonicated for 30 min at t =

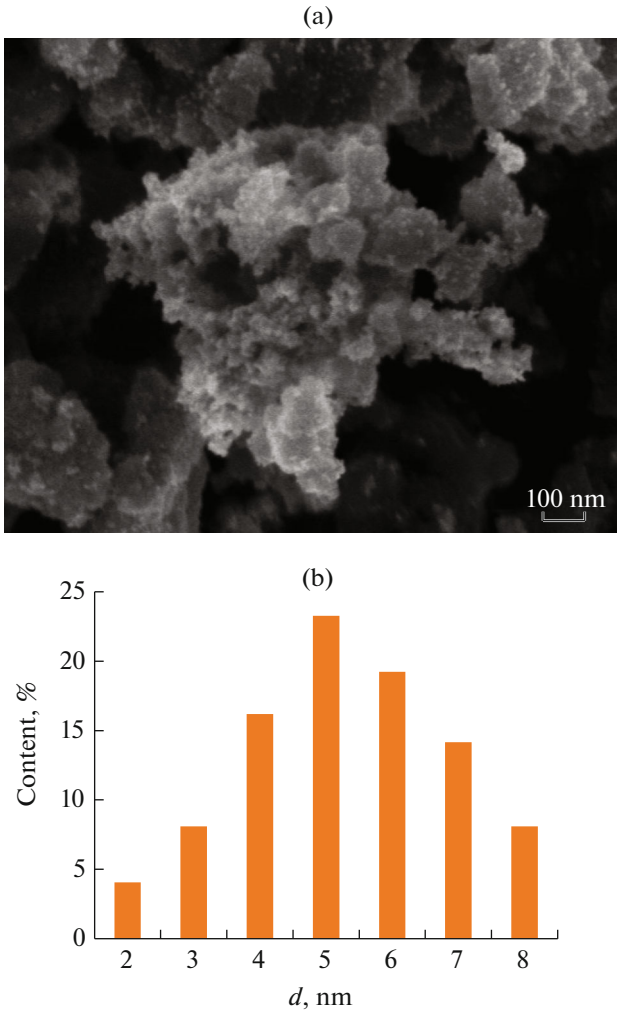

Fig. 3. (Color online) (a) Micrograph of a 10% Pt/TiO_2 sample and (b) the size distribution of platinum particles obtained from the analysis of micrographs.

30–40°C. An aliquot of 6 μL of the solution (60 μg of catalyst) was taken from the resulting suspension and applied to the electrode. The electrode was dried in air for 30 min. After complete drying of the prepared layer, the electrode was placed in a three-electrode electrochemical cell. Before measurements, the background electrolyte (0.5 M H_2SO_4) was saturated with oxygen for 2 h. The polarization curves of the ORR were recorded in the range of 1–0.2 V at a potential application rate of 5 mV/s in the cathode and anodic directions at an electrode rotation rate in the range of 600–3500 rpm.

The desorption of hydrogen, carbon monoxide, and copper adatoms were electrochemically studied in a standard three-electrode cell using a PI-50 Pro potentiostat (Elins, Russia). A glassy carbon disk was used as an operating electrode, a normal hydrogen electrode (NHE) was used as a reference electrode, relative to which all potentials were given, and a platinum foil was used as an auxiliary electrode. An electrolyte was 0.5 M H_2SO_4. All measurements were performed at room temperature.

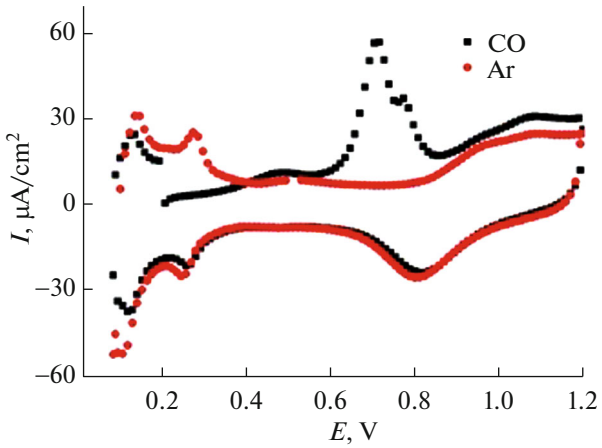

Fig. 4. (Color online) CVA of the background of the 20% Pt/TiO_2 anatase sample (S_{sp} = 216 m^2/g) (Ar atmosphere), carbon monoxide desorption curve. 0.5 M H_2SO_4, three-electrode liquid cell, glassy carbon electrode, 20 mV/s.

Studies in a FC were performed in an ElectroChem cell with a size of 2.2 × 2.2 cm. When assembling the membrane-electrode units, a Nafion® 212 membrane and a Freudenberg C8 gas-diffusion layer were used. The catalyst bed composition was 30% of Nafion®, 70% of an electrocatalyst for Pt/C materials and 5% of CNT, 17% of Nafion®, and 78% of an electrocatalyst for Pt/TiO_2 materials; in both cases, the platinum loading on the electrodes was about 0.5 mg/cm^2. The pressing was carried out at 130°C and a pressure of 80 kg/cm^2 for 3 min. A FC was tested at station G40 (Greenlight Innovation, USA). The current-voltage characteristics of FCs were measured using a P-400LX electronic load (Elins, Russia). Accelerated degradation tests were performed using cyclic voltammetry: 0.6–1.1 V, 0.1 V/s, 30000 H_2/Ar cycles, and RH = 100%. To control the degradation degree after 0, 1000, 5000, 10000, 20000, and 30000, the electrochemically active area of the platinum surface was measured using cyclic voltammetry: 0–1.2 V, 0.05 V/s, H_2/Ar, and RH = 100%. In addition, the power characteristics of the FC were measured at these points by measuring stationary curves in the potentiostatic mode [23].

To compare the obtained electrochemical characteristics of the materials, we used a 20% Pt/C commercial catalyst (Etek, USA).

RESULTS AND DISCUSSION

The stability of platinized oxide systems was studied by cyclic voltammetry (CVA) in the range 0.05–1.2 V. The obtained background curves (Fig. 5) have a

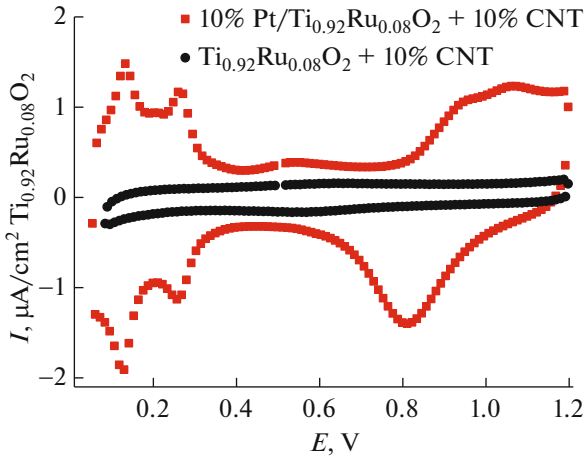

Fig. 5. (Color online) Background curves of 10% $Pt/Ti_{0.92}Ru_{0.08}O_{2-\delta}$ (rutile) + 10% CNT and $Ti_{0.92}Ru_{0.08}O_{2-\delta}$ (rutile) + 10% CNT. 0.5 M H_2SO_4, Ar, three-electrode liquid cell, glassy carbon electrode, 20 mV/s.

characteristic form for CVA of platinum in the background electrolyte: peaks on the anode branch are hydrogen desorption at 50–350 mV and oxygen adsorption at 800–1200 mV while peaks on the cathode branch are oxygen desorption at 600–1200 mV and hydrogen adsorption at 50–350 mV. The absence of obvious differences in CVA of pure platinum indicates resistance to electrooxidation and electroreduction of the resulting system in the studied potential range.

The most interesting from the viewpoint of use in fuel cells are electrocatalysts, on which the ORR proceeds according to a four-electron mechanism. In this case, hydrogen peroxide that is a strong oxidizing agent for the materials of the catalytic layer is not formed on the cathode. The rotating electrode method was used to study the ORR mechanism.

Studies in a cell with a rotating disk electrode (RDE) showed that the value of the limiting current depends on the rotation speed of the electrode. The effect of concentration polarization was taken into account using the Koutecky–Levich ratio, and the experimental data were compared with a commercially produced electrocatalyst 20% Pt/C Vulcan XC72:

$$1/i = 1/i_k + 1/Z\omega^{0.5} = 1/i_k + 1/i_D, \quad (2)$$

where i is the current at the disk electrode; i_k is the kinetic current; i_D is the diffusion current, mA/cm^2; and ω is the electrode rotation speed, rad/s;

$$Z = 0.62nFD^{2/3}\nu^{-1/6}c, \quad (3)$$

where n is the number of electrons participating in the electrochemical reaction; F is the Faraday number, C/mol; is the kinematic viscosity of the liquid, cm^2/s; c is the oxygen concentration in solution, mol/cm^3; and D is the diffusion coefficient, cm^2/s.

The ORR on platinum in an acidic medium is known to proceed predominantly according to the four-electron mechanism. Since the tangents of the slope of the straight lines equal to 1/Z in Fig. 7 at 0.3 V are close, this indicates that the ORR mechanism on Pt/TiO_2 is similar to that on Pt/C.

The catalytic activity of 20% Pt/TiO_2 is 1.1, 1.8 mA/cm^2 (35 ± 4.58 ± 6 μA/cm^2 Pt) at a potential of 0.9, 0.88 V, respectively; for 20% Pt/C Etek, the catalytic activity is 1.2, 2.1 mA/cm^2 (36 ± 4, 63 ± 6 μA/cm^2 Pt) at a potential of 0.9 and 0.88 V, respectively. The area of electrochemically active Pt on the studied electrodes was 31 ± 3 cm^2 Pt/cm^2 of the electrode for 20% Pt/TiO_2 and 33 ± 3 cm^{2}Pt/cm^2 of the electrode for 20% Pt/C Etek. Thus, 20% Pt/TiO_2 has an activity in the ORR that is within the experimental error close to that of 20% Pt/C Etek; similar data were obtained in [12].

Studies and comparison of the electrocatalytic activity of 20% Pt/C Etek and 20% Pt/TiO_2 + 5%

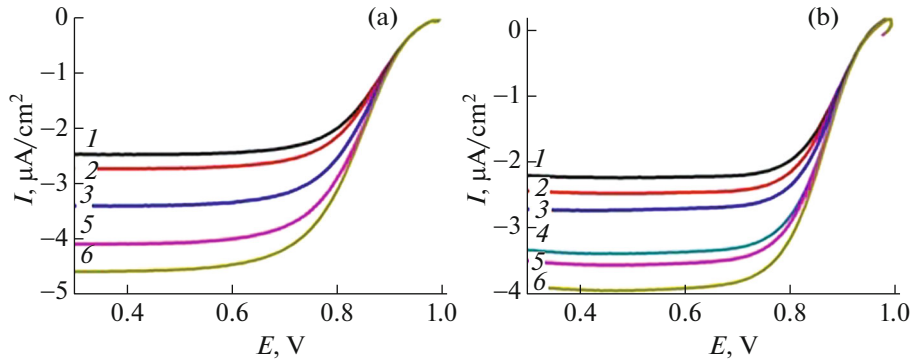

Fig. 6. (Color online) Polarization curves of the ORR on the (a) 20% Pt/TiO_2 + 5% CNT and (b) 20% Pt/C Vulcan XC72 catalyst, 25°C, ν = 5 mV/s, oxygen atmosphere, three-electrode liquid cell, NVE. The RDE rotation speed 1–6 corresponds to 84, 105, 147, 190, 210, and 263 rad/s.

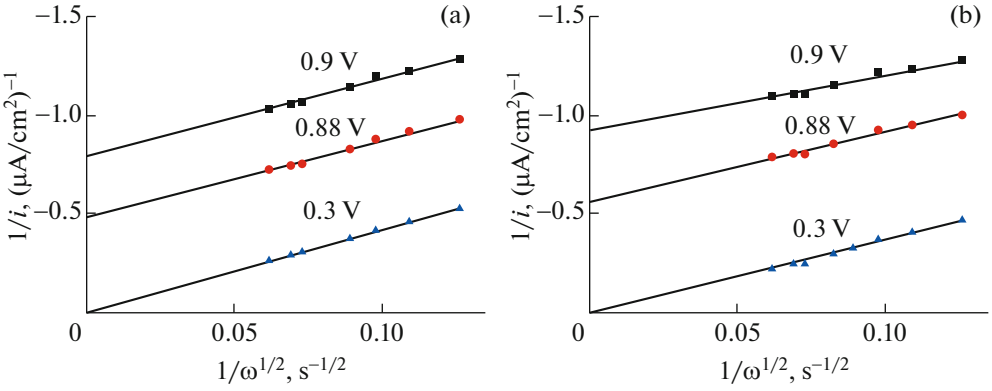

Fig. 7. (Color online) Dependences $1/i - 1/\omega^{-1/2}$ obtained at $E = 0.9$–0.3 V for (a) the 20% Pt/C Etek catalyst and (b) 20% Pt/TiO_2 + 5% CNT catalyst based on measured polarization curves.

CNT in a liquid half-cell showed that the structure of the oxide support affects the electrocatalytic activity of platinum in the ORR. For example, when using a TiO_2-based support with an anatase structure, the ORR rate is close to the rate of this reaction on 20% Pt/C Etek catalysts. At the same time, the ORR rate on catalysts using a TiO_2-based support with a rutile structure is significantly lower and increases with an increase in the degree of doping with ruthenium (Fig. 8). The reasons for the change in the electrocatalytic activity with a change in the structure and composition of the oxide support are most likely associated with a change in the rate of individual stages of oxygen electroreduction [24]. However, additional studies are required to confirm this. Due to the higher electrocatalytic activity of the material with a TiO_2-based support with an anatase structure, further studies of the efficiency of operation in FC and studies of the stability were performed only with this material.

Studies of electrocatalysts in model single fuel cells showed that the use of an electrocatalytic material based on 20% Pt/TiO_2 (anatase) + 5% CNTs allows providing a fuel cell operating efficiency comparable to that of the 20% Pt/C Etek commercial catalyst. However, in the case of catalysts based on 20% Pt/TiO_2 (anatase), the losses associated with diffusion hindrances in the catalytic layer begin to appear earlier than those for catalysts based on 20% Pt/C Etek (Fig. 9). Most likely, this is a consequence of insufficient optimization of the composition of the catalytic layer when using catalysts based on 20% Pt/TiO_2 (anatase). The density of TiO_2-based supports is significantly higher, and the hydrophobicity is significantly lower than that of supports based on carbon materials. This leads to the formation of denser catalytic layers, which are more prone to flooding with water formed during the fuel cell operation.

The stability of the 20% Pt/C Etek and 20% Pt/TiO_2 + 5% CNT catalysts was compared using the

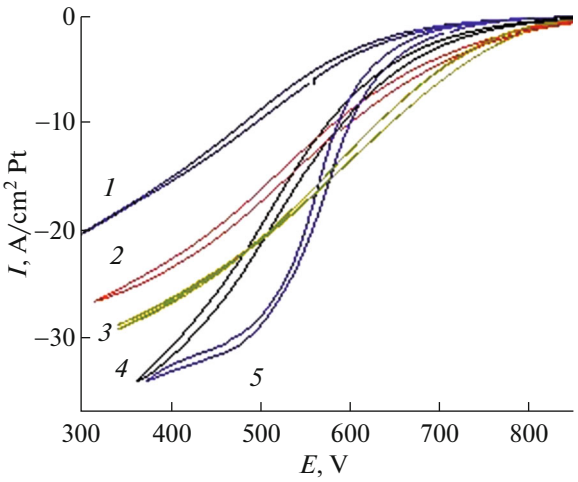

Fig. 8. (Color online) Data on the study of (*1*) 10% Pt/TiO_2 rutile, (*2*) 10% $Pt/Ti_{0.98}Ru_{0.02}O_2$, (*3*) Etek 20% Pt/C, (*4*) 10% $Pt/Ti_{0.97}Ru_{0.03}O_2$, and (5) 20% Pt/TiO_2 anatase electrocatalysts in a three-electrode gas-liquid half-cell.

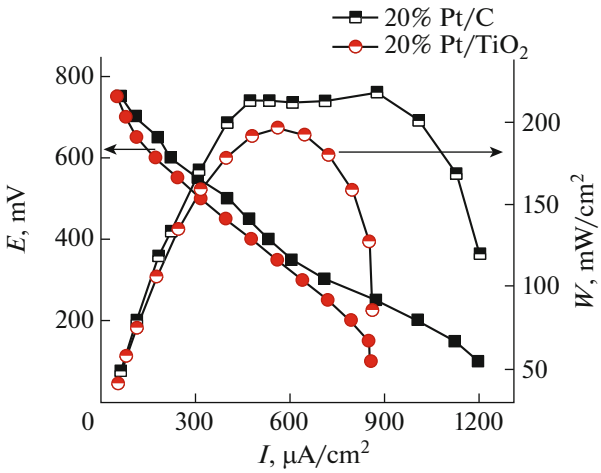

Fig. 9. (Color online) Current-voltage and power characteristics of fuel cells using 20% Pt/C Etek and 20% Pt/TiO_2 + 5% CNTs as catalysts.

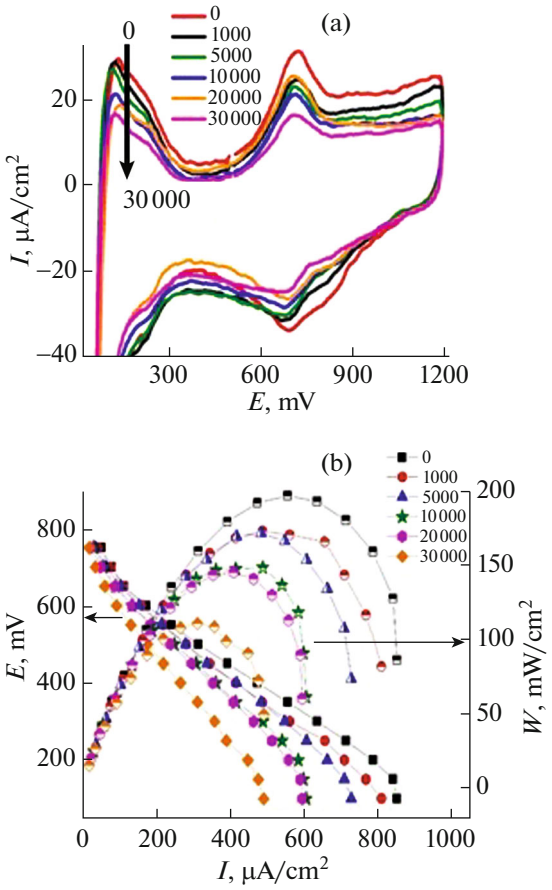

Fig. 10. (Color online) (a) CVA and (b) power characteristics of a fuel cell using a 20% Pt/TiO_2 + 5% CNT catalyst after a various number of degradation cycles.

accelerated FC degradation method [23, 25]. We used the accelerated degradation routine similar to that applied in [25], in which tests of the commercial catalyst HiSPEC 13100 (70Pt/C) in the potential range of 0.6–1.1 V 10000 cycles at a rate of 100 mV/s showed that the TE only has 20% of the initial power after accelerated aging.

Table 1. Comparison of residual currents in a fuel cell after different numbers of degradation cycles for 70% Pt/C HiSPEC 13100 and 20% Pt/TiO_2 (anatase) + 5% CNT catalysts

Number of degradation cycles	S_{H_2N}/S_{H_2O} 20%Pt/TiO_2	S_{H_2N}/S_{H_2O} 70%Pt/C HiSPEC 13100 [25]
0	1	1
1000	0.96	0.89
5000	0.88	0.56
10000	0.68	0.41
20000	0.62	
30000	0.52	

Degradation studies of catalysts 20% Pt/TiO_2 (anatase) + 5% CNTs showed that the developed catalyst is highly stable to oxidative degradation (Fig. 10) and is significantly (5–6 times) more stable than the commercial 70% Pt/C HiSPEC catalyst 13100 (data of [25]) (Table 1).

CONCLUSIONS

Catalysts with oxide supports in the $Ti_{1-x}Ru_xO_{2-\delta}$ system were studied. The mechanism of oxygen electroreduction on $Pt/Ti_{1-x}Ru_xO_{2-\delta}$ catalysts was shown to be similar to that on Pt/C catalysts: oxygen reduction proceeds mainly by the four-electron mechanism. However, the composition and structure of the oxide support affect the rates of individual stages of oxygen electroreduction, which leads to a change in the overall rate of the ORR. However, additional studies are required to confirm this.

The use of an electrocatalytic material based on 20% Pt/TiO_2 (anatase) + 5% CNT allows to provide a fuel cell efficiency comparable to that of the commercial 20% Pt/C Etek catalyst. However, in the case of catalysts based on 20% Pt/TiO_2 (anatase), losses associated with diffusion hindrances of oxygen transfer in the catalytic layer begin to manifest themselves earlier than for catalysts based on 20% Pt/C "Etek." This is due to a higher density and hydrophilicity of TiO_2-based supports than those of carbon-based supports. This leads to the formation of denser catalytic layers, which are more prone to flooding with water formed during the FC operation.

Research of the degradation processes of the 20% Pt/TiO_2 (anatase) + 5% CNT catalysts showed that the developed catalyst is highly stable to oxidative degradation and is 5–6 times more stable than the commercial 70% Pt/C HiSPEC 13100 catalyst.

ACKNOWLEDGMENTS

The work was carried out using the resources of the NTI Competence Center on Technologies for New and Mobile Energy Sources at the IPCP RAS and using the equipment of the Analytical Center for Collective Use of the IPCP RAS.

FUNDING

The work was partially carried out on the topic of the State assignment, state registration no. AAAA-A19-119061890019-5, temkart 0089-2019-007 and was supported by the Ministry of Science and Higher Education of the Russian Federation, agreement no. 05.605.21.0188 of December 3, 2019, RFMEFI60519X0188.

REFERENCES

1. N. Wagner, W. Schnurnberger, B. Mueller, and M. Lang, Electrochim. Acta **43**, 3785 (1998). https://doi.org/10.1016/S0013-4686(98)00138-8
2. I. A. Stenina, E. Y. Safronova, A. B. Yaroslavtsev, et al., Therm. Eng. **63**, 385 (2016). https://doi.org/10.1134/S0040601516060070
3. B. Wang, J. Power Sources **152**, 1 (2005). https://doi.org/10.1016/j.jpowsour.2005.05.098
4. Yu. Dobrovolsky, L. Leonova, and A. Vakulenko, Solid State Ionics **86**, 1017 (1996). https://doi.org/10.1016/0167-2738(96)00244-5
5. K. C. Neyerlin, R. Srivastava, C. Yu, and P. Strasser, J. Power Sources **186**, 261 (2009). https://doi.org/10.1016/j.jpowsour.2008.10.062
6. S. Mukerjee, S. Srinivasan, and M. P. Soriaga, J. Electrochem. Soc. **142**, 1409 (1995). https://doi.org/10.1149/1.2048590
7. R. C. Koffi, C. Coutanceau, E. Garnier, et al., Electrochim. Acta **50**, 4117 (2005). https://doi.org/10.1016/j.electacta.2005.01.028
8. S. Mukerjee, S. J. Lee, E. A. Ticianelli, et al., Electrochem. Solid-State Lett. **2**, 12 (1999). https://doi.org/10.1149/1.1390718
9. L. Frolova, N. Lyskov, and Yu. Dobrovolsky, Solid State Ionics **225**, 92 (2012). https://doi.org/10.1016/j.ssi.2012.02.013
10. C.-P. Lo and A. Kumar, ECS Trans. **33**, 493 (2010). https://doi.org/10.1149/1.3484547
11. M. Gutz and H. Wendt, Electrochim. Acta **43**, 3637 (1998). https://doi.org/10.1016/S0013-4686(98)00121-2
12. X. Liu, J. Chena, G. Liu, et al., J. Power Sources **195**, 4098 (2010). https://doi.org/10.1016/j.jpowsour.2010.01.077
13. B. Ruiz-Camacho, O. Martínez-Álvarez, H. H. Rodríguez-Santoyo, and V. Granados-Alejo, J. Electroanal. Chem. **725**, 19 (2014). https://doi.org/10.1016/j.jelechem.2014.04.019
14. B. Ruiz-Camacho, H. Martínez-González, R. G. González-Huerta, and M. Tuño-Velázquez, Int. J. Hydrogen Energy **39**, 16731 (2014). https://doi.org/10.1016/j.ijhydene.2014.02.109
15. L. A. Frolova and Yu. A. Dobrovolsky, Russ. Chem. Bull. **60**, 1101 (2011).
16. M. T. Colomer and J. R. Jurado, Chem. Mater. **12**, 923 (2000). https://doi.org/10.1021/cm9903879
17. A. A. Belmesov, A. A. Baranov, and A. V. Levchenko, Russ. J. Electrochem. **54**, 493 (2018). https://doi.org/10.1134/S1023193518060046
18. A. A. Bel'mesov, A. V. Levchenko, T. A. Palankoev, L. S. Leonova, A. E. Ukshe, A. I. Chikin, and N. G. Bukun, Russ. J. Electrochem. **49**, 831 (2013). https://doi.org/10.1134/S1023193513080053
19. A. S. Zyubin, T. S. Zyubina, Yu. A. Dobrovol'skii, A. A. Bel'mesov, and V. M. Volokhov, Russ. J. Inorg. Chem. **59**, 816 (2014). https://doi.org/10.1134/S0036023614080221
20. C. L. Green and A. Kucernak, J. Phys. Chem. B **106**, 1036 (2002). https://doi.org/10.1021/jp0131931
21. B. P. Tarasov, V. E. Muradyan, and A. A. Volodin, Russ. Chem. Bull. **60**, 1261 (2011). https://link.springer.com/content/pdf/10.1007/s11172-011-0194-8.pdf.
22. A. A. Volodin, A. A. Belmesov, and V. B. Murzin, Inorg. Mater. **49**, 656 (2013). https://doi.org/10.1134/S0020168513060174
23. V. B. Avakov, V. A. Bogdanovskaya, V. A. Vasilenko, B. A. Ivanitskii, E. M. Kol'tsova, A. V. Kuzov, A. V. Kapustin, I. K. Landgraf, M. M. Stankevich, and M. R. Tarasevich, Russ. J. Electrochem. **51**, 719 (2015).
24. M. Shao, Q. Chang, J.-P. Dodelet, and R. Chenitz, Chem. Rev. **116**, 3594 (2016). https://doi.org/10.1021/acs.chemrev.5b00462
25. U. S. Drive Fuel Cell Tech Team Cell Component Accelerated Stress Test and Polarization Curve Protocols for PEM Fuel Cells. http://energy.gov/sites/prod/files/2015/08/f25/fc-to_dwg_usdrive_fctt_accelerated_stress_tests_-jan2013.pdf. Accessed January 2013.

Translated by A. Ivanov